AGU PUBLICATIONS

Paleoceanography

RESEARCH ARTICLE
10.1002/2013PA002509

Key Points:
- Intensity of Indian monsoon is traced with geochemical and grain size analyses of sediments
- Fluvial versus aeolian sediment input to Arabian Sea mimics DO oscillations
- During Heinrich events the Indian monsoon weakened distinctly

Supporting Information:
- Readme
- Figure S1
- Figure S2
- Figure S3
- Figure S4
- Figure S5
- Figure S6

Correspondence to:
G. Deplazes,
gaudenz.deplazes@alumni.ethz.ch

Citation:
Deplazes, G., A. Lückge, J.-B. W. Stuut, J. Pätzold, H. Kuhlmann, D. Husson, M. Fant, and G. H. Haug (2014), Weakening and strengthening of the Indian monsoon during Heinrich events and Dansgaard-Oeschger oscillations, *Paleoceanography*, *29*, 99–114, doi:10.1002/2013PA002509.

Received 17 MAY 2013
Accepted 3 JAN 2014
Accepted article online 8 JAN 2014
Published online 18 FEB 2014

Weakening and strengthening of the Indian monsoon during Heinrich events and Dansgaard-Oeschger oscillations

Gaudenz Deplazes[1], Andreas Lückge[2], Jan-Berend W. Stuut[3,4], Jürgen Pätzold[3], Holger Kuhlmann[3], Dorothée Husson[3], Mara Fant[3], and Gerald H. Haug[1,5]

[1]Geological Institute, Department of Earth Sciences, ETH Zürich, Zürich, Switzerland, [2]Bundesanstalt für Geowissenschaften und Rohstoffe, Hannover, Germany, [3]MARUM-Center for Marine Environmental Sciences, Bremen University, Bremen, Germany, [4]NIOZ-Royal Netherlands Institute for Sea Research, Texel, The Netherlands, [5]DFG-Leibniz Center for Earth Surface Process and Climate Studies, Institute for Geosciences, Potsdam University, Potsdam, Germany

Abstract The Dansgaard-Oeschger oscillations and Heinrich events described in North Atlantic sediments and Greenland ice are expressed in the climate of the tropics, for example, as documented in Arabian Sea sediments. Given the strength of this teleconnection, we seek to reconstruct its range of environmental impacts. We present geochemical and sedimentological data from core SO130-289KL from the Indus submarine slope spanning the last ~80 kyr. Elemental and grain size analyses consistently indicate that interstadials are characterized by an increased contribution of fluvial suspension from the Indus River. In contrast, stadials are characterized by an increased contribution of aeolian dust from the Arabian Peninsula. Decadal-scale shifts at climate transitions, such as onsets of interstadials, were coeval with changes in productivity-related proxies. Heinrich events stand out as especially dry and dusty events, indicating a dramatically weakened Indian summer monsoon, potentially increased winter monsoon circulation, and increased aridity on the Arabian Peninsula. This finding is consistent with other paleoclimate evidence for continental aridity in the northern tropics during these events. Our results strengthen the evidence that circum-North Atlantic temperature variations translate to hydrological shifts in the tropics, with major impacts on regional environmental conditions such as rainfall, river discharge, aeolian dust transport, and ocean margin anoxia.

1. Introduction

Paleoproxy and climate-modeling studies have documented correspondences between tropical and high-latitudinal climate variability on various time scales [*Behl and Kennett*, 1996; *Schulz et al.*, 1998; *Peterson et al.*, 2000; *Wang et al.*, 2001; *North Greenland Ice Core Project Members*, 2004; *Zhang and Delworth*, 2005]. During the last glacial period, climate variability is characterized by millennial-scale warmer (interstadial) and colder (stadial) Dansgaard-Oeschger (DO) oscillations [*Bond et al.*, 1993; *Dansgaard et al.*, 1993]. Some of the colder DO oscillations coincide with anomalous occurrences of ice-rafted detritus in North Atlantic sediments, which are referred to as Heinrich events [*Heinrich*, 1988; *Hemming*, 2004]. It is postulated that instabilities of the Northern Hemisphere glacial ice sheets led to a freshwater input to the North Atlantic during Heinrich events, which caused a strong decrease or even shutdown of the Atlantic meridional overturning circulation (AMOC) [*Broecker*, 1994; *Ganopolski and Rahmstorf*, 2001; *McManus et al.*, 2004]. The DO oscillations and Heinrich events are also expressed in climate records of the Indo-Asian realm [*Schulz et al.*, 1998; *Wang et al.*, 2001; *Altabet et al.*, 2002; *Clemens and Prell*, 2003; *Higginson et al.*, 2004; *Wang et al.*, 2008; *Banakar et al.*, 2010]. However, forcing and response mechanisms of the Indo-Asian monsoon system in conjunction with these millennial-scale oscillations are still poorly understood [*Kudrass et al.*, 2001; *Caley et al.*, 2011].

Sedimentary archives in the northeastern Arabian Sea have been described as sensitive recorders of Indian monsoonal climate on annual to millennial time scales [*Schulz et al.*, 1998; *von Rad et al.*, 1999; *Lückge et al.*, 2002]. During the past years a controversial discussion evolved whether the mainly productivity-related proxies in the Arabian Sea reflect dominantly changes in the Indo-Asian monsoonal intensity or rather changes in the AMOC [*Pourmand et al.*, 2004; *Schmittner et al.*, 2007; *Böning and Bard*, 2009; *Ziegler et al.*, 2010; *Caley et al.*, 2011].

©2014. American Geophysical Union. All Rights Reserved.

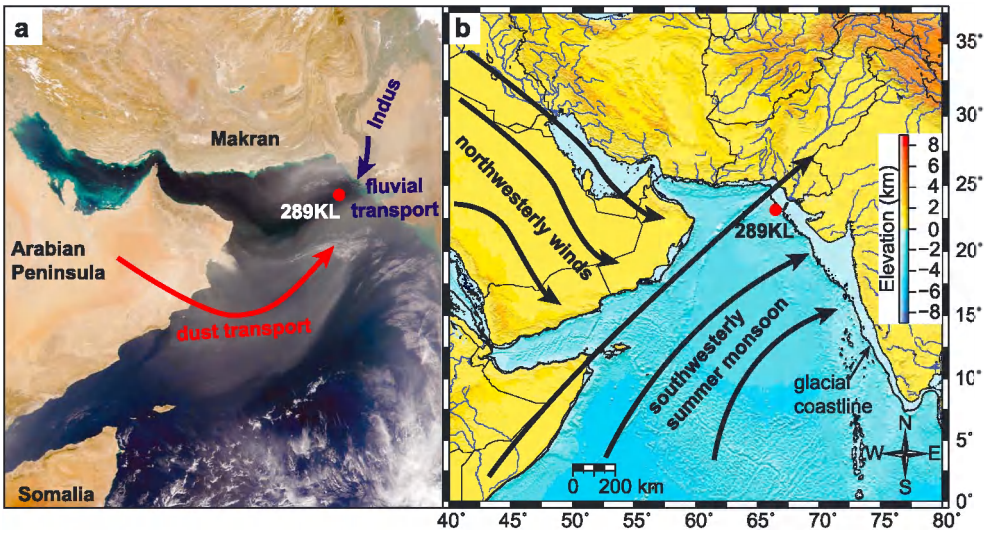

Figure 1. Environmental setting of sediment core SO130-289KL in the northeastern Arabian Sea. (a) SeaWiFS (Sea-viewing Wide Field-of-view Sensor) image of a storm transporting dust from the Arabian Peninsula to the Arabian Sea at 12 March 2000 (SeaWiFS project, NASA/Goddard Space Flight Center, Orbital Imaging Corporation (ORBIMAGE)). (b) Bathymetric map of the Arabian Sea and the Persian Gulf (geomorphologic data from General Bathymetric Chart of the Oceans 08). The bathymetric contour of 120 m is highlighted, which is approximating the coastline during maximum last glacial lowstand of sea level. The black arrows schematically indicate the wind field during early summer monsoon, which is favorable to transport dust from the Arabian Peninsula to the indicated core location [*Krishnamurti et al.*, 1980; *Sirocko and Sarnthein*, 1989].

In this study, we present a multiproxy record of sediment core SO130-289KL from the oxygen minimum zone (OMZ) in the northeastern Arabian Sea (Figure 1) in order to reconstruct monsoon-related climate and oceanic variability over the last 80 kyr in decadal- to centennial-scale resolution. Sediment total color reflectance (L^*) and total organic carbon (TOC) measurements are used to reconstruct marine productivity and organic matter preservation. Bulk chemical sediment analyses (X-ray fluorescence (XRF)) are applied to infer variations of biogenic and terrigenous input as well as their provenance. Grain size analyses and end-member modeling of siliciclastic grain size distributions are used to identify transport mechanisms of the sediments. The combination of high-resolution grain size and elemental analyses sheds new light on the interaction, chronology, and potential causalities between atmospheric and oceanographic driving mechanisms of sediment formation in the Arabian Sea in decadal- to centennial-scale resolution.

2. Modern Indian Monsoon

The modern seasonal cycle over the Arabian Sea is dominated by the Indian monsoon. In boreal summer (June–September) powerful southwesterly winds (Figure 1) are generated by the large pressure gradient between the Indian-Tibetan low-pressure cell and a belt of high pressure over the Southern Ocean [*Webster et al.*, 1998]. It is debated if the strong summer monsoon is mainly caused by elevated heating of the Tibetan plateau [*Wu et al.*, 2012] or rather by orographic insulation of warm, moist air over continental India from the cold and dry extratropics [*Boos and Kuang*, 2010]. In any case, the strong and moist monsoonal southwesterly winds, which are linked to the Intertropical Convergence Zone (ITCZ), provide intense rainfall to the Indian subcontinent. This leads, together with snowmelt in the Himalayas, to high runoff rates from the continent [*Bookhagen and Burbank*, 2010], which results in high terrigenous input to the coastal sediments near the Indus River mouth [*Milliman et al.*, 1984].

The Arabian Sea receives one of the highest amounts of dust input in the world [*Rea*, 1994]. The highest wind speeds and dust loads around the Arabian Sea are reached in spring and during the summer monsoon period [*Ackerman and Cox*, 1989; *Clemens*, 1998; *Schulte and Müller*, 2001]. In this season dust is mobilized in the northern Arabian Peninsula and around the Persian Gulf by northwesterly winds, which result from cyclonic circulation around the Asian low [*Middleton*, 1986; *Sirocko et al.*, 1993; *Clemens*, 1998]. These winds are referred to as Shamal in the Persian Gulf region. The dust transport is peaking during occasional major dust storms [*Ackerman and Cox*, 1989]. The dust-bearing, dry, and warm winds are lifted up and override the low-level, moist, and cooler southwesterly winds leading to a monsoonal inversion between the two air masses

©2014. American Geophysical Union. All Rights Reserved.

[*Findlater*, 1969]. The convergence of these winds forms the regional summer ITCZ. The northwesterly winds tend to turn east above the monsoon inversion [*Sirocko and Sarnthein*, 1989], and while lifting up, they drop most of their load, which is partly picked up by the low-level southwesterly wind resulting in a dust transport to the northeastern Arabian Sea (Figure 1).

The summer monsoon southwesterly winds trigger upwelling of nutrient-rich waters, particularly in the western Arabian Sea [*Honjo et al.*, 1999]. Enhanced nutrient supply to surface waters leads to extremely high productivity in the Arabian Sea during the summer monsoon. Subsequently, high remineralization rates of organic matter lead to a rapid consumption of oxygen and establish oxygen-depleted conditions in the water column and on the sea floor within the OMZ.

In boreal winter the land-sea pressure gradient is reverse and moderate, dry and cold northeastern winds flow from the Indian-Tibetan high-pressure zone toward the southward shifted ITCZ, which is located at about 10°S. Northeasterly winds induce convective mixing along the coast, generating a second, smaller productivity maximum in the northeastern Arabian Sea [*Reichart et al.*, 1998; *Kumar et al.*, 2000]. The winter monsoon is characterized by overall drier conditions and lower dust input into the Arabian Sea [*Sirocko and Lange*, 1991; *Clemens*, 1998; *Prins and Weltje*, 1999]. However, the western Himalayas, also part of the Indus River drainage basin, are strongly influenced by the westerlies during the winter. The westerlies bring moisture from the North Atlantic, Mediterranean, or other inland seas, which leads to high winter snow cover and subsequent snowmelt-runoff during spring [*Bookhagen and Burbank*, 2010].

3. Materials and Methods

3.1. Core Setting

Sediment core SO130-289KL (23°07.34'N, 66°29.84'E, 571 m water depth, Figure 1) was taken at the Sindh continental margin within the OMZ that expands today from about 200 to 1200 m water depth [*von Rad et al.*, 1999]. This 20.2 m long piston core was recovered on a levee at the flank of the Indus submarine canyon off the Indus River mouth. Oceanographic setting and sedimentology of the core setting of SO130-289KL and neighboring cores SO90-136KL and SO90-137KA have been described by, e.g., *Schulz et al.* [1998], *von Rad et al.* [1999], and *von Rad et al.* [2002].

3.2. Age Model

The first-order age model for SO130-289KL is based on 20 accelerator mass spectrometry ^{14}C dates and cross correlation to radiocarbon dated color records from the same region [*Deplazes et al.*, 2013]. The age model was further fine tuned by correlating the high-resolution total color reflectance (L^*) records to the ice core $\delta^{18}O$ record of North Greenland Ice Core Project (NGRIP) using the GICC05modelext age scale [*North Greenland Ice Core Project Members*, 2004; *Wolff et al.*, 2010]. Because of this fine tuning it is not possible to interpret lead or lag relationships between the two records although lead and lag relationships among the proxies measured from the same core are certainly valid. An additional time control point is given by the Toba Ash layer identified in core SO130-289KL at 18.43 m subbottom depth (Figure 2) [*Schulz et al.*, 2002; *von Rad et al.*, 2002; *Storey et al.*, 2012].

3.3. Lamination Index

A Lamination Index (LI) has been established and is similar to the Bioturbation Index of *Behl and Kennett* [1996] and *von Rad et al.* [1999]. A value of 4 characterizes undisturbed sediments with fine laminations (typically $<$ 1 mm to 2 mm thick). A value of 3 represents discontinuous or irregular laminations (typically 1 to 4 mm thick). A LI of 2 describes slightly to partly bioturbated sediments. A LI of 1 represents strongly to completely bioturbated or homogenous sediments. The LI is not defined on the entire cross-core length but on the 1.7 cm broad image transects of which the total color reflectance (L^*) was determined.

3.4. Total Organic Carbon (TOC)

Samples for TOC measurements were taken every 2 cm in the interval of 7.51 to 9.79 m core depth (115 samples). The sediment samples were dried and TOC was determined with a LECO CS-444 instrument by infrared detection after combustion at 1400°C. Prior to combustion, TOC samples were acid treated (10% HCl at 80°C) to remove inorganic carbon.

©2014. American Geophysical Union. All Rights Reserved.

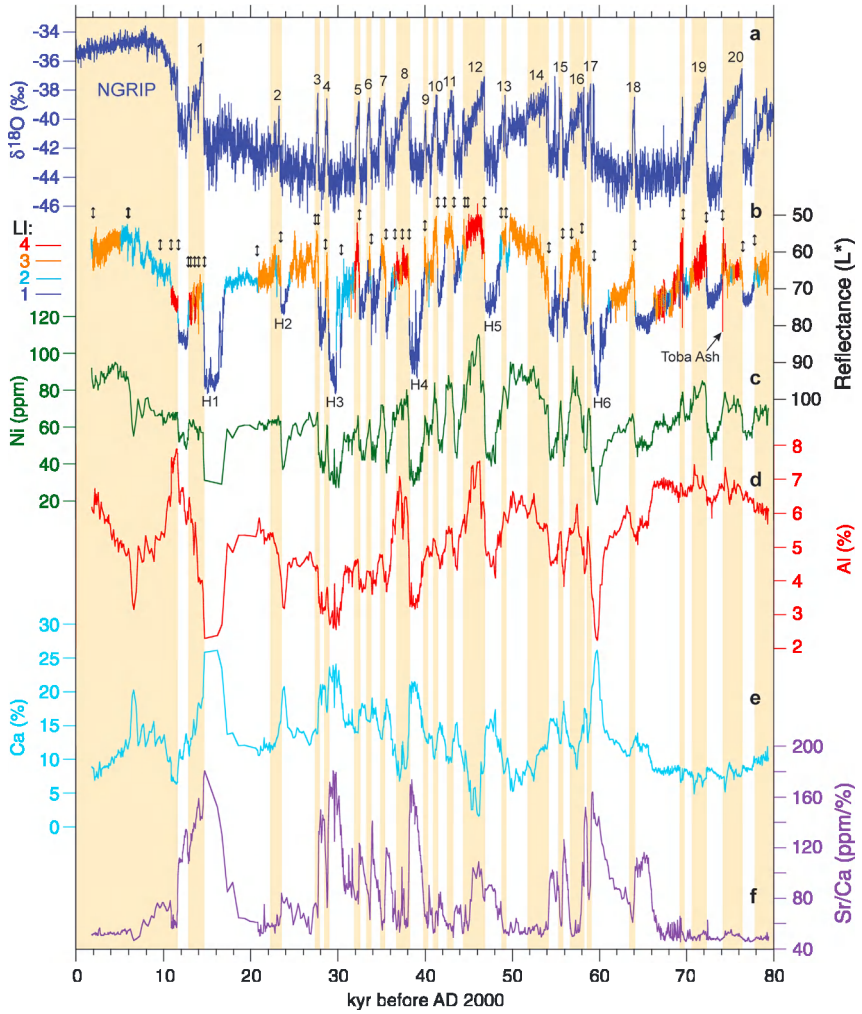

Figure 2. Comparison of color reflectance (*L**) and elemental abundances from the northeastern Arabian Sea (SO130-289KL) with NGRIP $\delta^{18}O$ ice core record. (a) NGRIP $\delta^{18}O$ record (dark blue) with 20 year resolution over the last 80 kyr [*Wolff et al.*, 2010]. (b) Sediment total reflectance (*L**) [*Deplazes et al.*, 2013] colored corresponding to the Lamination Index (LI). A LI of 4 indicates finely laminated sediments, a LI of 1 indicates homogenous or bioturbated sediments. Elemental concentrations of (c) nickel (green), (d) aluminum (red), (e) calcium (light blue), and (f) elemental ratio of strontium to calcium Sr/Ca (purple). Greenland interstadial numbers are indicated above, Heinrich events (H) below the *L** record. Double-headed arrows indicate stratigraphic tie points. Yellow shaded areas denote relatively warmer climates in the Northern Hemisphere.

3.5. Conventional XRF Measurements

Bulk chemical sediment analyses were performed on samples from almost every 2 cm over the entire 20.2 m long core (966 samples). This results in an average temporal sampling resolution of ~ 80 years over the entire core. The analyses were accomplished with X-ray fluorescence (XRF) using Philips PW 2400 and PW 1480 wavelength dispersive spectrometers. Forty-two major and trace elements were quantitatively analyzed after fusion of the samples with lithium metaborate at 1200°C for 20 min (sample/$LiBO_2$ = 1/5). Quality of the results was controlled with certified reference materials (i.e., Community Bureau of Reference, Brussels). The precision for major elements was generally better than ±0.5% and better than 5% for trace elements. Three outliers in the presented nickel (Ni) record have been removed from the record (3.58, 8.07, and 17.29 m).

3.6. Grain Size Analysis and End-Member Modeling

Grain size distributions were studied in 2 cm intervals in the upper half of the core (0.21–9.79 m, 474 samples parallel to XRF, Figure 3 and Figures S1–S4 in the supporting information). The samples were pretreated with H_2O_2 (30–35%), HCl (10%), and NaOH (6 g pellets dissolved in 100 mL H_2O) to separate the terrigenous

©2014. American Geophysical Union. All Rights Reserved.

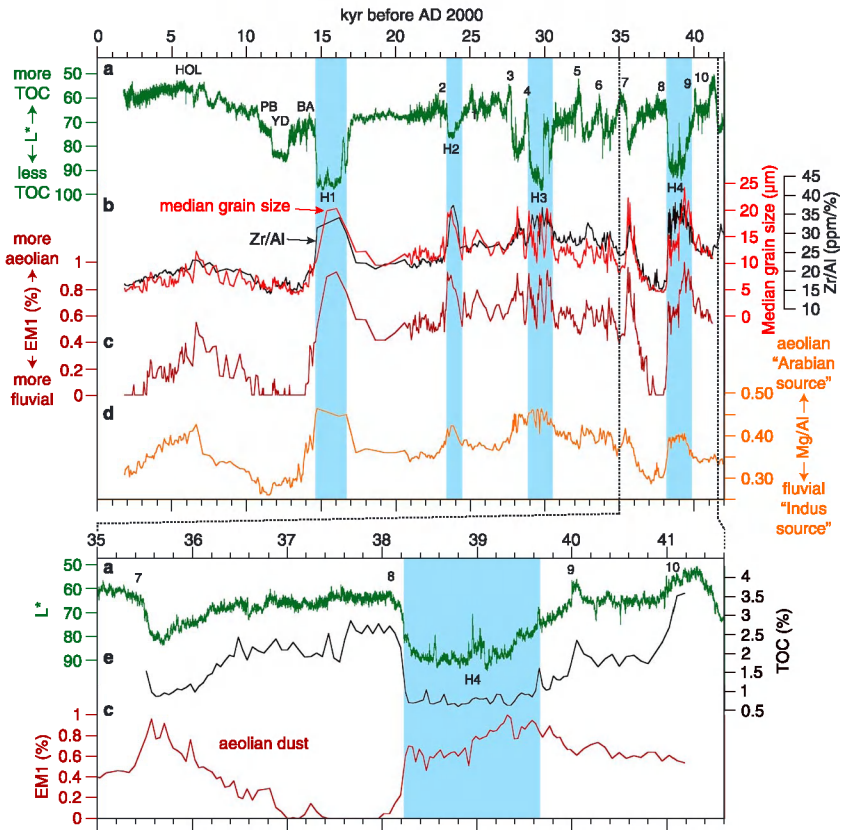

Figure 3. Comparison of color reflectance (*L**) with proxies tracing sediment composition, transport, and source over the (top) last 42 kyr and over the time interval of (bottom) 41.6–35.0 kyr before 2000 AD. (a) Sediment total reflectance (green). (b) Median grain size (red) and elemental ratio of zirconium to aluminum Zr/Al (black). (c) Grain size end-member EM1 as proxy for the coarser aeolian dust (maroon). (d) Elemental ratio of magnesium to aluminum Mg/Al (orange) as provenance indicator of the terrigenous sediment fraction (Figure 5). (e) Total organic carbon (TOC, black). Blue-shaded areas indicate Heinrich events 4 to 1. Greenland interstadial numbers are indicated above, Heinrich events (H) below the *L** record. Bølling-Allerød (BA), Younger Dryas (YD), Preboreal (PB), and Holocene (HOL) are assigned.

sediment fraction from organic carbon, calcium carbonate, and biogenic opal, respectively. The presented grain size measurements reflect therefore only variations within the siliciclastic fraction. To prevent formation of aggregates $Na_4P_2O_7 \times 10\ H_2O$ was added prior to grain size analysis. Grain size analyses were performed on a laser diffraction particle size analyzer (Beckman Coulter) LS200, resulting in 92 size classes from 0.4 to 2000 µm.

An inversion algorithm for end-member (EM) modeling was applied to unmix the polymodal grain size distributions that are composed of sediment subpopulations resulting from different transport mechanisms [*Weltje*, 1997; *Prins and Weltje*, 1999; *Prins et al.*, 2000] (Figures S1–S4). The 2-EM and 4-EM models capture the dominantly bimodal grain size distributions best. The 4-EM has a mean coefficient of determination of 89.7%, i.e., the end-member model reproduces on average 89.7% of the input variances [*Prins and Weltje*, 1999; *Stuut et al.*, 2002]. The 2-EM has coefficient of determination of 64.7%. In spite of the lower coefficient of determination a 2-EM model was selected for the investigated intervals, because of the principle of parsimony (a minimal number of end-members) and a reasonable attribution of end-members to particular mechanisms of transport.

4. Results

4.1. Facies and Chemical Composition of Sediments

The sediments of core SO130-289KL are characterized by two sedimentary facies during the last glacial period. During interstadials the sediments are dark colored and distinctly to indistinctly laminated; during stadials and Heinrich (equivalent) events they are light colored and in general homogenous or bioturbated.

©2014. American Geophysical Union. All Rights Reserved.

The L^* record and Lamination Index (LI) trace these changes with low L^* and high LI values during the interstadials and vice versa during stadials (Figure 2). Heinrich events are characterized by light-colored sediments having highest L^* values in the entire record.

Two similar, alternating facies can be found at the beginning of the current interglacial period (Figures 2 and 3). The sediments of the Bølling-Allerød (BA) are dark colored and finely to discontinuously laminated, whereas the sediments of the Younger Dryas (YD) are white colored and bioturbated. The sediments from the "Preboreal" (PB, 11.7–10.9 kyr) are unique within the entire record and consist of finely laminated sediments with a reddish color. The Holocene sediments are dark colored. The early to mid-Holocene sediments are slightly to partly bioturbated, whereas the middle to late Holocene sediments are discontinuously laminated.

Sediment-color properties have been used in this region as a proxy for TOC (%) [*Schulz et al.*, 1998]. This is in line with the observation that the L^* record shows a remarkable similarity to the new TOC measurements in the interval of 41 to 35.5 kyr before 2000 AD (Figure 3e). A polynomial regression of second order of L^* (smoothed over 2 cm) to TOC (%) revealed a coefficient of determination R^2 of 0.9. The TOC content is generally lower in stadials and Heinrich events than in the interstadials and varies between 0.6% in Heinrich event 4 and up to 3.6% in the Interstadial 10.

The L^* record is also mimicked by the concentration of the trace element nickel (Ni). Ni is delivered to the sediment mainly in association with organic matter [*van der Weijden et al.*, 2006] and underlines that the L^* record traces the organic matter content over the entire record.

In the time period of ~ 81 to 68 kyr before 2000 AD (mainly end of Marine Isotope Stage (MIS) 5, *Lisiecki and Raymo* [2005]) element concentrations of terrigenous, siliciclastic origin (e.g., Al, Fe, K, Si, Ti, and Zr) reproduce the DO oscillations traced by the L^* and Ni records only partly and show a reduced amplitude in their variability (Figures 2 and S5). In contrast, during most of the last glacial period (~ 68–14 kyr, mainly MIS 4–2) the terrigenous element concentrations mimic the DO oscillations traced by the L^* and Ni records. From 13 to 2 kyr before 2000 AD elements of terrigenous origin show again a different, temporarily opposite pattern compared to the L^* and Ni records. The $CaCO_3$ content, traced by calcium (Ca) concentrations, shows a pattern that is inverse to the siliciclastic element concentrations. In summary, the sediment consists mainly of $CaCO_3$, a siliciclastic fraction and organic carbon; biogenic opal is rare ($<$ 1%) [*von Rad et al.*, 1999].

Elements of siliciclastic origin were additionally plotted normalized to Al to investigate changes in the chemical composition related to transport mechanisms or provenance of the terrigenous sediments that are not depending on dilution by other sedimentary constituents [*Lückge et al.*, 2001]. Terrigenous element ratios such as Ti/Al, Mg/Al, and Zr/Al are neither depending on redox nor on productivity changes and show similar, inverse millennial- to centennial-scale variability patterns as the terrigenous element concentrations (Figures 3, S5, and S6). The element ratio of Sr/Ca follows in general the pattern of Ca (%) (Figure 2).

4.2. Grain Size Analysis

The median grain size record of the terrigenous fraction over the last 41 kyr shows in general higher values during the end of the last glacial period and lower values during the current interglacial period (Figure 3). The absolute values vary between ~ 4 and 24 μm. On millennial-scale, the median grain size record shows a pattern concomitant with the DO oscillations as defined by the L^* record with low values during interstadials, higher values during stadials, and highest values during Heinrich events. At prominent climate transitions, such as at the onset of Interstadial 8, the median grain size shows abrupt changes, which are coeval with changes in L^*, in element concentrations and in element to Al ratios (Figure 3). The "two-end-member (EM) model" is in accordance with the median grain size record. The end-members EM1 and EM2 have modal grain sizes of ~ 22.5 μm and ~ 4.7 μm (Figure S3). The element ratio of Zr/Al traces the general pattern in the median grain size and 2-EM model in great detail (Figure 3b).

5. Discussion

5.1. Paleoproductivity and OMZ Intensity

Total color reflectance (L^*) [*Deplazes et al.*, 2013] and Ni (%) show a similar millennial- to centennial-scale pattern similar to paleoclimate records from Greenland [*North Greenland Ice Core Project Members*, 2004; *Wolff et al.*, 2010] (Figure 2), North Atlantic [*Bond et al.*, 1993], and from the Indo-Asian realm [e.g., *Wang et al.*, 2001].

©2014. American Geophysical Union. All Rights Reserved.

The millennial-scale variability characterized by DO oscillations and intercalated Heinrich events has been recognized at several locations documented by different proxies in the Arabian Sea [*Schulz et al.*, 1998; *Altabet et al.*, 2002; *Clemens and Prell*, 2003; *Ivanochko et al.*, 2005]. However, at least three hypotheses were proposed which describe the imprint of millennial- to orbital-scale climate oscillations in Arabian Sea sediments.

The first hypothesis assigns the dominant role to the Indian southwest summer monsoon [*Schulz et al.*, 1998; *Schulte and Müller*, 2001; *Altabet et al.*, 2002; *Clemens and Prell*, 2003; *Caley et al.*, 2011]. A strong southwest summer monsoon leads to coastal and open-ocean upwelling of nutrient-rich subsurface waters mostly in the western Arabian Sea causing high productivity in large parts of the Arabian Sea. High surface water productivity leads to high export production and high oxygen demand driven by remineralization of organic matter and ultimately to anoxic conditions hampering bioturbation and potentially enhancing preservation of organic matter. Accordingly, *Clemens and Prell* [2003] used mainly proxies that are potentially productivity related (δ^{15}N, opal mass accumulation rate (MAR), percent *Globigerina bulloides*, excess Ba MAR, and lithogenic grain size) to define the Arabian Sea Summer Monsoon stack (SM stack).

In the second hypothesis, the productivity and intensity of the OMZ in the northern Arabian Sea are not only determined by the summer monsoon but also by an interplay of summer and winter monsoon elements. During stadials and Heinrich events enhanced northeastern monsoonal winds lead to winter mixing and intermediate water formation down to at least 600 m water depth resulting in weaker OMZ conditions [*Reichart et al.*, 1998; *Reichart et al.*, 2004; *Klöcker and Henrich*, 2006]. In contrast, interstadials are characterized by productivity maxima and shallow winter mixing.

The third hypothesis describes productivity and OMZ intensity changes as a function of changes in the AMOC. The intensity of the OMZ might be influenced by changes in the formation of Subantarctic Mode Water and Antarctic Intermediate Water (SAMW-AAIW) [*Schulte et al.*, 1999; *Pichevin et al.*, 2007; *Böning and Bard*, 2009]. Stable isotope studies on planktonic and benthic foraminifera off Somalia suggest enhanced intermediate water supply to the northern Indian Ocean when the AMOC was reduced [*Jung et al.*, 2009]. Intensified northeastward injection of oxygen-rich SAMW-AAIW would lead to increased ocean ventilation and decreased intensity of the OMZ during stadials and Heinrich events compared to interstadials. However, climate-model simulations of oxygen and nutrient concentrations during the last glacial period suggest that changes in consumption are more important than ventilation in the Arabian Sea [*Schmittner et al.*, 2007]. According to these model simulations, reduced AMOC conditions lead to a decreased nutrient delivery to the upper Indo-Pacific Ocean, reducing productivity and causing a reduced OMZ intensity as a consequence of reduced oxygen consumption. The model, however, does not reproduce the strong OMZ conditions in the Arabian Sea.

In our study the DO oscillations and the current interglacial period are traced in high resolution by the *L** record and Ni (%) that show a high correlation with organic matter contents. Organic petrographic analyses indicate that the organic matter is predominantly of marine origin [*Lückge et al.*, 1999, 2012]. The observed signal cannot be the result of dilution by carbonate or siliciclastic contents as they show a different pattern, for example, during the deglaciation. The *L** record could in principle reflect OMZ intensity and therefore represent a preservation rather than a productivity signal. The Sr/Ca record (Figure 2) that has been interpreted as an aragonite dissolution record [*Reichart et al.*, 1998; *Klöcker and Henrich*, 2006; *Böning and Bard*, 2009] and therefore as an OMZ intensity proxy follows, in general, the *L** oscillations. However, surface sediment studies from the Oman and Pakistan margins suggest that bottom water oxygen concentration is not solely driving the amount of buried organic matter [*Cowie et al.*, 2009]. Instead, a high settling flux of organic matter (i.e., high export productivity in the surface water) [*Pedersen et al.*, 1992] seems to be needed. The basic question whether the different proxies reflect mainly primary productivity or bottom water oxygen concentration or a combination of both (i.e., oxygen exposure time) [*Sinninghe Damsté et al.*, 2002] has been a matter of debate since several decades [*Tyson*, 2005]. It is difficult to separate these two mechanisms because they are intrinsically correlated. This means that increased productivity can directly influence the oxygen concentration of the bottom waters. The correspondence of our *L** record with Arabian Sea SM stack [*Clemens and Prell*, 2003] (Figure S6) and results of previous studies linking the observed Northern Hemisphere millennial-scale pattern to productivity proxies in the Arabian Sea [*Reichart et al.*, 1998; *von Rad et al.*, 1999; *Sinninghe Damsté et al.*, 2002; *Pourmand et al.*, 2004] suggest, however, that monsoonal driven productivity plays a major but not an exclusive role in determining the *L** and organic matter record.

©2014. American Geophysical Union. All Rights Reserved.

5.2. Terrestrial Siliciclastic Signature and Depositional Regime

Climate variations in monsoon winds and precipitation influence not only the deposition of biogenic (as traced by L^*) but also of lithogenic sedimentary components. Therefore, geochemical composition and properties of the siliciclastic fraction that are independent of productivity or OMZ intensity but dependent on fluvial or aeolian input were analyzed. Since the L^* measurements and the geochemical analyses were performed in the same core and in high resolution the records can be compared on a time scale of on average ~80 years and in case of the onset of Interstadial 8 even in a resolution of ~40–60 years.

Element concentrations of siliciclastic, terrigenous origin like Al (%) closely follow the DO pattern over most of the presented glacial record (Figures 2 and S5). Warmer interstadials correlate with higher siliciclastic concentrations than colder stadials. Element ratios like Ti/Al, Mg/Al, and Zr/Al, which are not influenced by productivity or redox conditions, follow a similar pattern like Ti- and Mg-element concentrations (Figures S5 and S6). This indicates that the millennial-scale pattern in the siliciclastic fraction is not just a result of dilution by biogenic carbonate input or preservation but reflects a change in input, source, or transport conditions. The changes in the Ti/Al, Mg/Al, and Zr/Al records are as abrupt and concomitant with changes in the L^* record (Figure 3).

In contrast, signals derived from the terrigenous fraction younger than 14–13 kyr before 2000 AD show another—partly opposite—pattern compared to the L^* record. Sedimentary studies have shown that off the large Indus River mouth most of the terrigenous sediments are transported from the delta to the deep-sea fan via large submarine canyon channel systems bypassing the continental slope [*von Rad and Tahir*, 1997]. The modern Indus submarine canyon starts about 3.5 km off the coast in about 20 m water depth and deepens seaward. At the shelf break region (135 m) the Indus submarine canyon has a maximum depth of about 1030 m [*Giosan et al.*, 2006; *Inam et al.*, 2007]. Therefore, the continental margin outside the Indus submarine canyon gets mostly covered by hemipelagic sediments with only few turbidites [*von Rad and Tahir*, 1997]. During sea level lowstands, like toward the end of the last glacial period, most of the fluvial sediments were deposited in channel-levee complexes of the Indus submarine fan, frequently in the form of turbidites [*Prins and Postma*, 2000]. During deglacial sea level rise, the deposition of turbidites decreased strongly on the Indus submarine fan leading to increased sedimentation in near-shore zones [*Prins and Postma*, 2000; *Prins et al.*, 2000] and possibly on the continental slope because of mobilization and reworking of sedimentary material [*von Rad et al.*, 1999]. This shift in depositional regime and redirection of sediment transport could explain the observed high terrigenous portion from the Bølling-Allerød to the onset of the Holocene associated with a maximum siliciclastic deposition in the reddish clays of the Preboreal (Figure 3). This time interval coincides with meltwater pulse MWP-1a and partly with MWP-1b representing periods of maximum eustatic sea level rise [*Stanford et al.*, 2011] (Figure 4). During the Holocene the terrigenous signal reflects nearly the opposite trend expected for summer monsoon conditions [*Fleitmann et al.*, 2003; *Gupta et al.*, 2003], which might reflect enhanced sediment deposition within the delta and a change in depositional regime on the continental shelf [*Limmer et al.*, 2012]. Today, sediments are mainly deposited within the innermost shelf and at the delta, whereas the outer shelf ($>$ ~90 m) is characterized by a lack of deposition [*von Rad and Tahir*, 1997]. The most recent evolution of sediment transport by the Indus River is additionally influenced by extensive damming in the catchment area [*Milliman et al.*, 1984; *Clift et al.*, 2008; *Lückge et al.*, 2012].

The onset of significant changes in the depositional regime and sediment provenance seems to have occurred at ~14 to 13 kyr before 2000 AD corresponding to a "threshold" sea level stand of ~70–80 m (Figure 4). It seems that the L^* record and the terrigenous signature follow tightly the DO oscillations and the SM stack (Figure S6) when the sea level was lower than ~70–80 m below the modern sea level (Figure 4). By analogy with present-day seasonal variations, warmer and more humid interstadials are expected to be characterized by elevated snowmelt and precipitation leading to high erosion and river sediment loads. This agrees with the observed enhanced contribution of siliciclastic material during the interstadials. The terrigenous sediment pattern is opposite to the SM stack or shows a considerably reduced millennial-scale variability when the sea level was above ~70–80 m during the time periods of ~80–68 and $<$ 14 kyr. We interpret that the siliciclastic oscillations reflect monsoon variability during most of the last glacial period [*North Greenland Ice Core Project Members*, 2004]. Before and after this time period they are influenced by a complex interplay of changes in provenance, depositional regime, and monsoon intensity.

©2014. American Geophysical Union. All Rights Reserved.

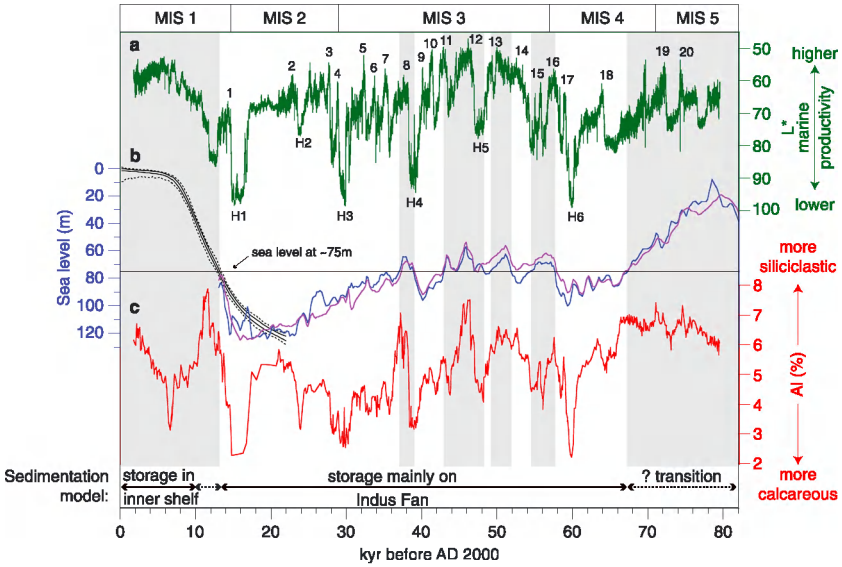

Figure 4. Comparison of Arabian Sea proxies and sea level. (a) Sediment total reflectance record (L^*, green). Greenland interstadial numbers are indicated above, Heinrich events (H) below the L^* record. MIS indicates Marine Isotope Stage [*Lisiecki and Raymo*, 2005]. (b) Highest-probability sea level history (black) based on six key deglacial sea level records over the last 22 kyr [*Stanford et al.*, 2011]. The black and dashed lines show the 99% and 95% confidence intervals, respectively. Sea level reconstruction from northern Red Sea for 82–13 kyr before 2000 AD based on benthic $\delta^{18}O$ considering two temperature corrections: in dark blue the alkenone sea surface temperatures as a maximum assumption for deep water temperature changes (benthic T_{max}) and in purple constant temperatures as a minimum approach (benthic T_{min}) [*Arz et al.*, 2007]. (c) Aluminum (red). Grey-shaded areas indicate time intervals in which the sea level was higher than ~75 m. The sedimentation model indicates changes in the depositional regime depending on the sea level.

5.3. Fluvial Versus Aeolian Signature

The siliciclastic input into the Arabian Sea can be of fluvial or aeolian origin. As the core location is near the Indus River delta, most of the terrigenous fraction is expected to be of fluvial origin [*von Rad et al.*, 1999]. Grain size analysis and end-member modeling are valuable tools to distinguish between sediments of aeolian and of fluvial origin in the Arabian Sea [*Prins and Weltje*, 1999]. At the continental slope off the Indus River delta, the fluvial fraction is characterized by finer grain sizes, because the coarser size fraction is either deposited in the delta or funneled within the submarine canyon [*Giosan et al.*, 2006; *Inam et al.*, 2007]. In contrast, the aeolian fraction has relatively coarser grain size distributions [*Prins and Weltje*, 1999; *Prins and Postma*, 2000]. Based on this basic premise and previous studies [*Prins and Weltje*, 1999; *Prins and Postma*, 2000] the coarser EM1 is assigned as aeolian dust and the finer EM2 as fluvial mud (Figures 3 and S3). The absolute values of the EM have to be interpreted with caution and give only qualitative estimations of the aeolian versus fluvial contributions.

The grain size analyses over the last 41 kyr generally show increased aeolian contribution (EM1) during the end of the last glacial and enhanced fluvial contribution (EM2) during the interglacial period (Figure 3). This is in line with previous results from continental, marine, and ice core studies that show elevated dust loads during the last glacial period [*Sirocko and Lange*, 1991; *Pourmand et al.*, 2004; *Ruth et al.*, 2007; *Roberts et al.*, 2011; *Sun et al.*, 2012].

On a millennial-scale, grain size analyses show a distinct increase of coarser aeolian dust (EM1) during Heinrich events 4 to 1 (Figure 3). In contrast, interstadials are characterized by fluvial mud (EM2) and coarser-grained aeolian dust (EM1) is nearly absent. This trend is clearly expressed during Heinrich event 4 and the subsequent Interstadial 8 (Figure 3). The measured median grain size record can be extended over the entire record by using Zr/Al as a grain size proxy. Zirconium is commonly associated with the coarser-grained heavy minerals [*von Rad et al.*, 1999; *Dypvik and Harris*, 2001], and Zr/Al is tracing the measured median grain size record in great detail (Figure 3). The Zr/Al ratio suggests that Heinrich events and stadials are consistently characterized by coarser grain sizes throughout the entire record (Figure S6).

©2014. American Geophysical Union. All Rights Reserved.

The grain size analyses strongly support the interpretation that the interstadials were more humid and warmer leading to enhanced deposition of fluvial mud (EM2), whereas the stadials and especially the Heinrich events were drier and colder leading to enhanced deposition of aeolian dust (EM1). The relative contribution of the coarser aeolian dust (EM1) abruptly decreases from a high percentage to 0% at the transition from Heinrich event 4 to Interstadial 8 (Figure 3). This change in dust contribution appears to have occurred within less than ~ 60 years. It is important to note that this change happens exactly at the time when the L^* record and TOC (%) are recording the abrupt onset of Interstadial 8. This is indicating that there is no lead or lag relation between abrupt atmospheric changes traced by grain size analysis and marine productivity traced by L^* record and TOC (%) on a decadal-scale. It is noteworthy that these transitions seem to occur in less than 100 years. This is ~ 200–300 years faster than modeled oxygen concentration changes due to changes in AMOC intensity [*Schmittner et al.*, 2007]. However, studies of the modern oceanic circulation suggest that, for example, changes in the formation of AAIW can be communicated within decades to the Arabian Sea [*Fine et al.*, 2008]. The observed synchronicity between grain size, L^*, and other compositional proxies suggests a dominant role of the monsoons for the oceanographic conditions and sediment formation in the Arabian Sea. Though it is likely that the oceanographic changes in the Arabian Sea were, especially on a longer time scale, also influenced by oscillations in SAMW-AAIW formation [*Schmittner et al.*, 2007; *Jung et al.*, 2009].

The inferred higher export productivity during interstadials is classically explained with increased nutrient availability by upwelling or changes in the oceanic current system, which are related to the southwest summer monsoon [e.g., *Schulz et al.*, 1998]. The observed multiproxy pattern could alternatively or additionally indicate increased nutrient injection via the Indus River provoking enhanced marine productivity in the region that is influenced by the Indus River plume and subsequent sediment deposition. The importance of fluvial nutrient delivery on coastal productivity at the study site has been suggested for recent times [*Lückge et al.*, 2012] and for other locations on various time scales [*Peterson et al.*, 2000; *Dagg et al.*, 2004]. The importance of riverine nutrient delivery during glacial times might have been underestimated in the northeastern Arabian Sea.

5.4. Provenance of Aeolian Dust

The Arabian Sea is surrounded by deserts in India, Pakistan, Iran, Iraq, and the Arabian Peninsula that are all potential sources of aeolian dust [*Sirocko and Lange*, 1991; *Pourmand et al.*, 2004]. Mineralogical and chemical studies of sediment samples from the Arabian Sea indicate that magnesium can be used as a potential provenance indicator of the Arabian Peninsula over the last 24 kyr [*Sirocko et al.*, 2000]. The distribution of Mg-rich minerals in the sediments shows a persistent pattern with a maximum close to the Arabian Peninsula and decreasing values in the more distal part of the Arabian Sea [*Sirocko and Lange*, 1991; *Sirocko et al.*, 2000]. This has been interpreted as deposition of dust plumes that are rich in Mg-bearing minerals. Palygorskite (Mg-rich clay) that can be found in sabkhas and Mesozoic rocks of the Arabian Peninsula or dolomite that is formed today in coastal sabkhas around the Persian Gulf are potential source-typical minerals [*Sirocko and Lange*, 1991; *Sirocko et al.*, 1993]. In contrast to Mg, Al reveals low concentrations in the sediments off the Arabian Peninsula [*Sirocko et al.*, 2000]. Accordingly, *Prins et al.* [2000] proposed that the excess of Mg to Al, i.e., Mg/Al and Ti/Al values of sediment samples, can be used to distinguish an aeolian "Arabian source" from a fluvial "Indus River source." In this study it was also shown that Mg/Al seems to not reflect grain size at the Indus submarine fan and the Oman continental slope.

The Mg/Al record of SO130-289KL shows a millennial-scale pattern similar to the aeolian end-member EM1 derived from the grain size analyses (Figures 3 and S6). A cross plot of Mg/Al versus Ti/Al indicates that sediments deposited during Heinrich events rather have an Arabian source signature, whereas interstadials rather have an Indus River source signature (Figure 5).

The Mg/Al record in general increases toward the end of the last glacial period, which suggests an increased relevance of the Arabian source. This long-term trend could partly be related to the lowering of the eustatic sea level leading to an exposure of the Persian Gulf, which represents a potential source of Mg-rich minerals [*Sirocko et al.*, 1993]. At the end of the last glacial period the sea level was ~ 120 m lower than today, so that the Persian Gulf was largely exposed (Figure 1b). However, the observed millennial-scale oscillations of Mg/Al are likely not reflecting changes in sea level fluctuations but rather changes in monsoonal climate variability,

©2014. American Geophysical Union. All Rights Reserved.

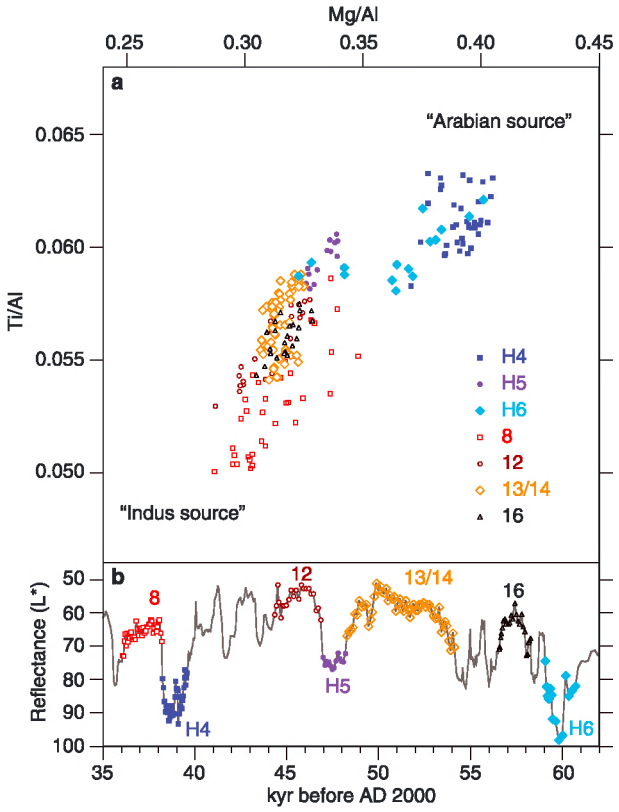

Figure 5. Provenance of terrigenous sediments deposited during major interstadials (reddish) and Heinrich events (bluish) over the time interval of 62–35 kyr. (a) Cross plot of elemental ratios of magnesium to aluminum Mg/Al and titanium to aluminum Ti/Al to trace the source of the terrigenous sediment from the Arabian Peninsula (aeolian) versus Indus River as shown in *Prins et al.* [2000]. (b) Sediment total reflectance (L^*) record with indicated samples used to characterize the major interstadials and Heinrich events in Figure 5a.

because the sea level seems not to fluctuate as abruptly as the above described proxies [*Arz et al.*, 2007; *Siddall et al.*, 2008].

It was previously postulated that in times of weakened summer monsoon the winter monsoon strengthened [*Reichart et al.*, 1998; *Sun et al.*, 2012] and that this could have led to increased aeolian input from the northeastern deserts like the Thar Desert [*Prins and Weltje*, 1999]. Based on the presented data an additional input cannot be excluded but the Mg/Al record suggests that such an input was not important enough to overprint, for example, the high Mg/Al values associated with Heinrich events, which are typical for an Arabian Peninsula provenance. Additionally, studies in the Thar Desert showed that during the last glacial period there was no major dune formation and that dust transport seems to depend mainly on the strength of the southwest summer monsoon [*Kar et al.*, 2001; *Glennie et al.*, 2002].

5.5. Climate Implication for the Arabian-Indian Realm

The grain size and geochemical analyses are consistently indicating that the interstadials during the last glacial period were characterized by an increased contribution of fluvial mud from the Indus River to the Arabian Sea (Figures 3 and S6). The Indus River discharge depends on rainfall and snowmelt [*Bookhagen and Burbank*, 2010]. This trend is therefore suggesting that warmer and more humid climate conditions in association with an intensified summer monsoon in the Indus River catchment area led to increased snowmelt and precipitation resulting in increased erosion and river sediment loads. This trend could be additionally strengthened by a weakened Indian winter monsoon and an increased westerly (winter) circulation, leading to increased snowfall and subsequent snowmelt in the western Himalayas. In contrast, the colder climate states are characterized by a relative increase of aeolian dust from the Arabian Peninsula.

Dust mobilization and transport from the Arabian Peninsula to the Arabian Sea have been interpreted in terms of continental aridity, wind strength, wind directions, and provenance [*Clemens*, 1998; *Prins and Weltje*, 1999;

©2014. American Geophysical Union. All Rights Reserved.

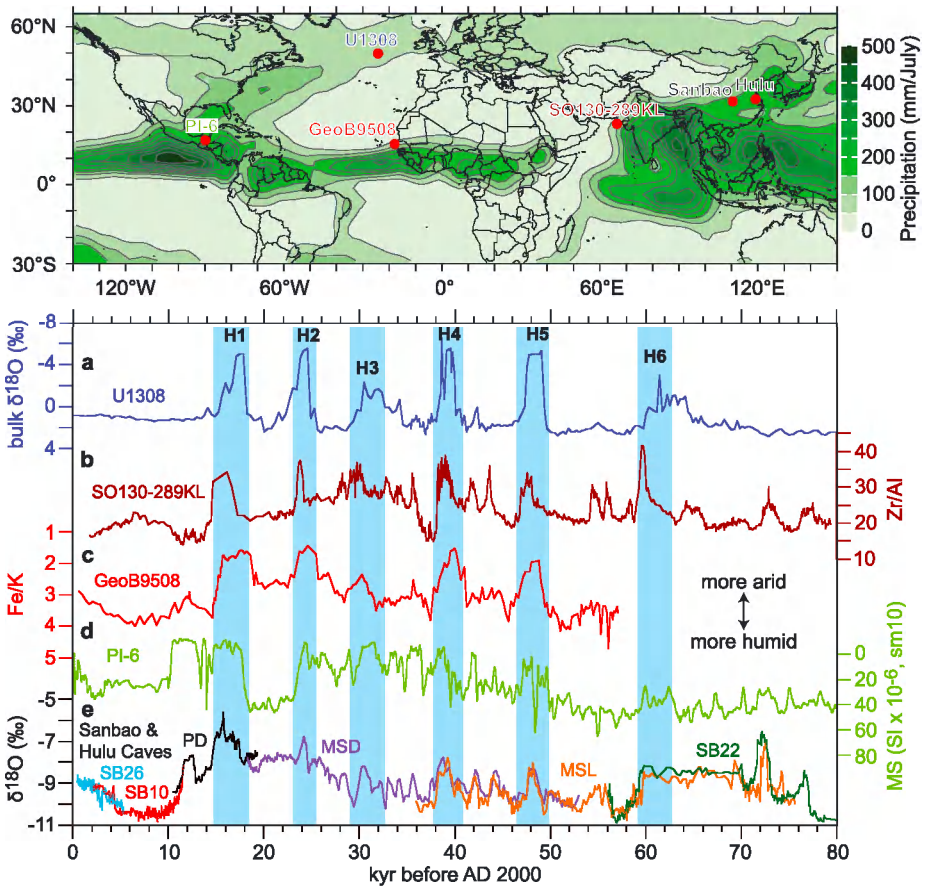

Figure 6. Co-occurrence of Heinrich events and increased aridity or decreased precipitation intensity reconstructed at different sites in the northern (sub) tropics. (top) The core locations of (bottom) the proxy records. Green coloring shows the distribution of average rainfall in July over the period of 1979 to 1995 [*Janowiak and Xie*, 1999]. (a) Bulk carbonate $\delta^{18}O$ record (dark blue) at IODP Site U1308 tracing Heinrich events in the North Atlantic [*Hodell et al.*, 2008a]. (b) Elemental ratio of zirconium to aluminum Zr/Al (maroon) from the northeastern Arabian Sea (this study) reflecting grain size, source aridity, and wind strength. (c) Elemental ratio of iron to potassium Fe/K (red) at core GeoB9508 off Senegal tracing Sahel aridity [*Mulitza et al.*, 2008]. (d) Magnetic susceptibility (MS, light green) at site PI-6 in the Lake Péten Itzá reflecting wet-dry cycles [*Hodell et al.*, 2008b]. (e) Stalagmites $\delta^{18}O$ records from Hulu Cave (PD, black; MSD, purple; MSL, orange) [*Wang et al.*, 2001] and Sanbao Cave (SB26, light blue; SB10, red; SB22, dark green) [*Wang et al.*, 2008] reflecting the intensity of the East Asian monsoon. For comparison, the Hulu $\delta^{18}O$ record is plotted 1.6‰ more negative to account for the higher Hulu values than Sanbao Cave [*Wang et al.*, 2008].

Pourmand et al., 2004]. Increased wind strength leads to an increase of the transported terrigenous grain sizes, whereas the total amount of transported dust seems to reflect mainly source aridity on the Arabian Peninsula [*Clemens and Prell*, 1990; *Rea*, 1994; *Clemens*, 1998]. The observed increase in aeolian contribution and grain size in core SO130-289KL could therefore reflect increased wind strength of the northwesterly winds in Mesopotamia and around the Persian Gulf and/or decreased summer monsoon-ITCZ intensity over the Arabian Peninsula, i.e., increased dust source aridity. This is in line with continental climate reconstructions, which propose a strengthening of the Shamal [*Glennie et al.*, 2002] and increased aridity on the Arabian Peninsula during colder climates [*Preusser et al.*, 2002; *Rosenberg et al.*, 2011]. The ITCZ-summer monsoon system might not only have decreased in intensity but might also have shifted southeastward during colder climate states, triggered by the increased strength of the northwesterly winds and a decreased strength of the southwesterly monsoonal winds. Dune reconstructions from the northeastern Arabian Peninsula (Wahiba Sands) stand in contrast to a major shift of the ITCZ near the ground during the last glacial period [*Preusser et al.*, 2002]. However, at higher tropospheric levels the strengthened northwesterly winds might have penetrated farther to the east, leading to higher dust entrainment to the study site.

5.6. Heinrich Events Related Droughts in the Tropical Northern Hemisphere

Heinrich events in the northeastern Arabian Sea stand out as especially prominent peaks of aeolian dust contribution, which suggest a strong reduction of precipitation in the Indus River catchment area and

©2014. American Geophysical Union. All Rights Reserved.

increased aridity on the Arabian Peninsula (Figure 3). For comparison, we analyzed a set of key paleoclimate records that is located at the northern rim of the modern boreal summer ITCZ position and therefore react most sensitively on a southward migration, contraction, and/or intensity decrease of the ITCZ monsoonal rain belt (Figure 6).

Mulitza et al. [2008] used the element ratio of Fe/K to reconstruct relative contributions of atmospheric dust and fluvial suspension in marine sediments close to the mouth of the Senegal River (Figure 6c). They found abrupt onsets of arid conditions in West African Sahel coinciding with Heinrich events. *Hodell et al.* [2008b] analyzed magnetic susceptibility in Lake Péten Itzá, Guatemala, which traces alternations between clay and gypsum deposition reflecting wet-dry cycles (Figure 6d). The most arid conditions were observed during Heinrich events, which is in line with reconstructions from the Cariaco Basin [*Peterson et al.*, 2000; *Deplazes et al.*, 2013]. *Wang et al.* [2001, 2008] found evidence for reduced East Asian monsoon intensity coinciding with Heinrich events by analyzing $\delta^{18}O$ in stalagmites from Hulu and Sanbao Caves (Figure 6e).

Heinrich events are characterized by increased freshwater input and cold temperatures in the North Atlantic [*Hodell et al.*, 2008a] (Figure 6a) and a reduction of the AMOC [*McManus et al.*, 2004]. Climate simulations indicate an ITCZ southward shift and a decrease in ITCZ summer monsoon intensity after a major reduction of the AMOC [*Zhang and Delworth*, 2005; *Krebs and Timmermann*, 2007]. *Stager et al.* [2011] have postulated that Heinrich event 1 coincided with a catastrophic drought in the tropical Afro-Asian region and *Schefuss et al.* [2011] have reported an ITCZ southward shift over southern Africa. Our study suggests together with a set of key paleoclimate records that the continental northern tropics around the globe were indeed impacted by increased aridity, but not only during Heinrich event 1 but also during Heinrich events 6 to 2. This indicates that the hypothesized effect of Heinrich events on the tropical hydroclimate occurred under a variety of background conditions (greenhouse gas concentrations, ice sheet extent, and insolation) during the last glacial period.

6. Conclusion

Elemental and grain size analyses indicate independently a high sensitivity of the studied site to monsoonal climate variability during the last glacial period. Our decadal- to centennial-scale Arabian Sea data suggest

1. The sedimentary depositional system at the continental slope off Pakistan seems to change with a "threshold" sea level of ~ 70–80 m. Fluvial suspended load is mainly transported along the Indus submarine canyon to the deep sea when sea level is lower than this threshold (~ 68–14 kyr). During this time interval, inorganic properties of the hemipelagic sediments closely trace millennial-scale climate variability. The deposition center of sedimentation shifts from the deep sea toward the shelf and delta when the sea level is higher than ~ 70–80 m, which leads to reduced climate sensitivity of inorganic properties at the study site.
2. The fluvial versus aeolian sedimentary contribution varies during the last glacial period in concordance with the Dansgaard-Oeschger oscillations. Interstadials are characterized by a fluvial signature indicating warmer and more humid glacial conditions leading to enhanced runoff and transport of suspended load by the Indus River to the ocean. Stadials reveal an increased aeolian contribution that at least partly originates from the Arabian Peninsula. This leads to the conclusion that colder climates were characterized by decreased ITCZ-Indian summer monsoon intensity and by increased northwesterly wind strength and aridity over the Arabian Peninsula. Heinrich events 6 to 1 stand out as prominent, especially dry and dusty events.
3. The abrupt and coeval change of inorganic, organic, oceanic, and atmospheric proxies at major climate transitions, e.g., the beginning of Interstadial 8, suggests a dominant role of the Indian summer monsoon on the oceanographic conditions and on subsequent sediment deposition in the Arabian Sea during MIS 3. Productivity-related proxies of the Arabian Sea (L^*, TOC) can therefore be interpreted in terms of monsoonal climate variability.
4. The close relationship between Indus River sediment and marine organic matter contributions during the last glacial period indicates that regional productivity was at least partially fed by fluvial nutrient injection.
5. Finally, this study together with other key paleoclimate records suggests increased continental aridity in the northern tropics during Heinrich events 6 to 1. Circum-North Atlantic temperature variations translate to hydrological shifts in the tropics, with major impacts on regional environmental conditions in the monsoonal world.

©2014. American Geophysical Union. All Rights Reserved.

Acknowledgments
We are thankful to Frank Korte for conducting the XRF analyses. We acknowledge Wiebke Keil, Ursula Röhl, Georg Scheeder, and Thomas Westerhold for technical assistance. We also thank A. Nele Meckler and Alfredo Martínez-Garcia for valuable discussions. We are thankful to S. Clemens for his helpful suggestions to improve the manuscript. Mara Fant and Dorothée Husson were supported through a MARUM Summer Student Fellowship. We acknowledge the Bundesministerium für Bildung und Forschung (BMBF, Bonn) for funding the SO130 cruise (project 03G0130A).

References

Ackerman, S. A., and S. K. Cox (1989), Surface weather observations of atmospheric dust over the southwest summer monsoon region, *Meteorol. Atmos. Phys.*, *41*(1), 19–34.

Altabet, M. A., M. J. Higginson, and D. W. Murray (2002), The effect of millennial-scale changes in Arabian Sea denitrification on atmospheric CO_2, *Nature*, *415*(6868), 159–162.

Arz, H. W., F. Lamy, A. Ganopolski, N. Nowaczyk, and J. Pätzold (2007), Dominant Northern Hemisphere climate control over millennial-scale glacial sea-level variability, *Quat. Sci. Rev.*, *26*(3-4), 312–321.

Banakar, V. K., B. S. Mahesh, G. Burr, and A. R. Chodankar (2010), Climatology of the Eastern Arabian Sea during the last glacial cycle reconstructed from paired measurement of foraminiferal $\delta^{18}O$ and Mg/Ca, *Quat. Res.*, *73*(3), 535–540.

Behl, R. J., and J. P. Kennett (1996), Brief interstadial events in the Santa Barbara basin, NE Pacific, during the past 60 kyr, *Nature*, *379*(6562), 243–246.

Bond, G., W. Broecker, S. Johnsen, J. McManus, L. Labeyrie, J. Jouzel, and G. Bonani (1993), Correlations between climate records from North Atlantic sediments and Greenland ice, *Nature*, *365*(6442), 143–147.

Böning, P., and E. Bard (2009), Millennial/centennial-scale thermocline ventilation changes in the Indian Ocean as reflected by aragonite preservation and geochemical variations in Arabian Sea sediments, *Geochim. Cosmochim. Acta*, *73*(22), 6771–6788.

Bookhagen, B., and D. W. Burbank (2010), Toward a complete Himalayan hydrological budget: Spatiotemporal distribution of snowmelt and rainfall and their impact on river discharge, *J. Geophys. Res.*, *115*, F03019, doi:10.1029/2009JF001426.

Boos, W. R., and Z. Kuang (2010), Dominant control of the South Asian monsoon by orographic insulation versus plateau heating, *Nature*, *463*(7278), 218–222.

Broecker, W. S. (1994), Massive iceberg discharges as triggers for global climate change, *Nature*, *372*(6505), 421–424.

Caley, T., B. Malaize, S. Zaragosi, L. Rossignol, J. Bourget, F. Eynaud, P. Martinez, J. Giraudeau, K. Charlier, and N. Ellouz-Zimmermann (2011), New Arabian Sea records help decipher orbital timing of Indo-Asian monsoon, *Earth Planet. Sci. Rev.*, *308*(3–4), 433–444.

Clemens, S. C. (1998), Dust response to seasonal atmospheric forcing: Proxy evaluation and calibration, *Paleoceanography*, *13*(5), 471–490.

Clemens, S. C., and W. L. Prell (1990), Late Pleistocene variability of Arabian Sea summer monsoon winds and continental aridity: Eolian records from the lithogenic component of deep-sea sediments, *Paleoceanography*, *5*(2), 109–145.

Clemens, S. C., and W. L. Prell (2003), A 350,000 year summer-monsoon multi-proxy stack from the Owen ridge, Northern Arabian sea, *Mar. Geol.*, *201*(1–3), 35–51.

Clift, P. D., et al. (2008), Holocene erosion of the Lesser Himalaya triggered by intensified summer monsoon, *Geology*, *36*(1), 79–82.

Cowie, G. L., S. Mowbray, M. Lewis, H. Matheson, and R. McKenzie (2009), Carbon and nitrogen elemental and stable isotopic compositions of surficial sediments from the Pakistan margin of the Arabian Sea, *Deep Sea Res., Part II*, *56*(6–7), 271–282.

Dagg, M., R. Benner, S. Lohrenz, and D. Lawrence (2004), Transformation of dissolved and particulate materials on continental shelves influenced by large rivers: Plume processes, *Cont. Shelf Res.*, *24*(7–8), 833–858.

Dansgaard, W., et al. (1993), Evidence for general instability of past climate from a 250-kyr ice-core record, *Nature*, *364*(6434), 218–220.

Deplazes, G., et al. (2013), Links between tropical rainfall and North Atlantic climate during the last glacial period, *Nat. Geosci.*, *6*(2), 213–217.

Dypvik, H., and N. B. Harris (2001), Geochemical facies analysis of fine-grained siliciclastics using Th/U, Zr/Rb and (Zr plus Rb)/Sr ratios, *Chem. Geol.*, *181*(1–4), 131–146.

Findlater, J. (1969), A major low-level air current near the Indian Ocean during the northern summer, *Q. J. R. Meteorol. Soc.*, *95*(404), 362–380.

Fine, R. A., W. M. Smethie, J. L. Bullister, M. Rhein, D. H. Min, M. J. Warner, A. Poisson, and R. F. Weiss (2008), Decadal ventilation and mixing of Indian Ocean waters, *Deep Sea Res., Part I*, *55*(1), 20–37.

Fleitmann, D., S. J. Burns, M. Mudelsee, U. Neff, J. Kramers, A. Mangini, and A. Matter (2003), Holocene forcing of the Indian monsoon recorded in a stalagmite from Southern Oman, *Science*, *300*(5626), 1737–1739.

Ganopolski, A., and S. Rahmstorf (2001), Rapid changes of glacial climate simulated in a coupled climate model, *Nature*, *409*(6817), 153–158.

Giosan, L., S. Constantinescu, P. D. Clift, A. R. Tabrez, M. Danish, and A. Inam (2006), Recent morphodynamics of the Indus delta shore and shelf, *Cont. Shelf Res.*, *26*(14), 1668–1684.

Glennie, K. W., A. K. Singhvi, N. Lancaster, and J. T. Teller (2002), Quaternary climatic changes over Southern Arabia and the Thar Desert, India, in *Tectonic and Climatic Evolution of the Arabian Sea Region*, edited by P. D. Clift et al., pp. 301–316, Geological Society, London.

Gupta, A. K., D. M. Anderson, and J. T. Overpeck (2003), Abrupt changes in the Asian southwest monsoon during the Holocene and their links to the North Atlantic Ocean, *Nature*, *421*(6921), 354–357.

Heinrich, H. (1988), Origin and consequences of cyclic ice rafting in the Northeast Atlantic Ocean during the past 130,000 years, *Quat. Res.*, *29*(2), 142–152.

Hemming, S. R. (2004), Heinrich events: Massive Late Pleistocene detritus layers of the North Atlantic and their global climate imprint, *Rev. Geophys.*, *42*, RG1005, doi:10.1029/2003RG000128.

Higginson, M. J., M. A. Altabet, D. W. Murray, R. W. Murray, and T. D. Herbert (2004), Geochemical evidence for abrupt changes in relative strength of the Arabian monsoons during a stadial/interstadial climate transition, *Geochim. Cosmochim. Acta*, *68*(19), 3807–3826.

Hodell, D. A., J. E. T. Channell, J. H. Curtis, O. E. Romero, and U. Röhl (2008a), Onset of "Hudson Strait" Heinrich events in the eastern North Atlantic at the end of the middle Pleistocene transition (similar to 640 ka)?, *Paleoceanography*, *23*, PA4218, doi:10.1029/2008PA001591.

Hodell, D. A., et al. (2008b), An 85-ka record of climate change in lowland Central America, *Quat. Sci. Rev.*, *27*(11-12), 1152–1165.

Honjo, S., J. Dymond, W. Prell, and V. Ittekkot (1999), Monsoon-controlled export fluxes to the interior of the Arabian Sea, *Deep Sea Res., Part II*, *46*, 1859–1902.

Inam, A., P. D. Clift, L. Giosan, A. R. Tabrez, M. Tahir, M. M. Rabbani, and M. Danish (2007), The geographic, geological and oceanographic setting of the Indus River, in *Large Rivers: Geomorphology and Management*, edited by A. Gupta, pp. 333–345, John Wiley & Sons, Ltd., New York.

Ivanochko, T. S., R. S. Ganeshram, G. J. A. Brummer, G. Ganssen, S. J. A. Jung, S. G. Moreton, and D. Kroon (2005), Variations in tropical convection as an amplifier of global climate change at the millennial scale, *Earth Planet. Sci. Rev.*, *235*(1-2), 302–314.

Janowiak, J. E., and P. P. Xie (1999), CAMS-OPI: A global satellite-rain gauge merged product for real-time precipitation monitoring applications, *J. Clim.*, *12*(11), 3335–3342.

Jung, S. J. A., D. Kroon, G. Ganssen, F. Peeters, and R. Ganeshram (2009), Enhanced Arabian Sea intermediate water flow during glacial North Atlantic cold phases, *Earth Planet. Sci. Rev.*, *280*(1-4), 220–228.

Kar, A., A. K. Singhvi, S. N. Rajaguru, N. Juyal, J. V. Thomas, D. Banerjee, and R. P. Dhir (2001), Reconstruction of the late Quaternary environment of the lower Luni plains, Thar Desert, India, *J. Quat. Sci.*, *16*(1), 61–68.

Klöcker, R., and R. Henrich (2006), Recent and Late Quaternary pteropod preservation on the Pakistan shelf and continental slope, *Mar. Geol.*, *231*(1–4), 103–111.

©2014. American Geophysical Union. All Rights Reserved.

Krebs, U., and A. Timmermann (2007), Tropical air-sea interactions accelerate the recovery of the Atlantic Meridional Overturning Circulation after a major shutdown, *J. Clim.*, *20*(19), 4940–4956.

Krishnamurti, T. N., Y. Ramanathan, R. Pasch, and P. Greiman (1980), Quick look Summer MONEX atlas*Rep.*, Florida State University, Tallahassee.

Kudrass, H. R., A. Hofmann, H. Doose, K. Emeis, and H. Erlenkeuser (2001), Modulation and amplification of climatic changes in the Northern Hemisphere by the Indian summer monsoon during the past 80 k.y, *Geology*, *29*(1), 63–66.

Kumar, S. P., M. Madhupratap, M. D. Kumar, M. Gauns, P. M. Muraleedharan, V. V. S. S. Sarma, and S. N. De Souza (2000), Physical control of primary productivity on a seasonal scale in central and eastern Arabian Sea, *Proc. Indian Acad. Sci., Earth Planet. Sci.*, *109*(4), 433–441.

Limmer, D. R., P. Böning, L. Giosan, C. Ponton, C. M. Köhler, M. J. Cooper, A. R. Tabrez, and P. D. Clift (2012), Geochemical record of Holocene to Recent sedimentation on the Western Indus continental shelf, Arabian Sea, *Geochem. Geophys. Geosys.*, *13*, Q01008, doi:10.1029/2011GC003845.

Lisiecki, L. E., and M. E. Raymo (2005), A Pliocene-Pleistocene stack of 57 globally distributed benthic $\delta^{18}O$ records, *Paleoceanography*, *20*, PA1003, doi:10.1029/2004PA001071.

Lückge, A., M. Ercegovac, H. Strauss, and R. Littke (1999), Early diagenetic alteration of organic matter by sulfate reduction in Quaternary sediments from the northeastern Arabian Sea, *Mar. Geol.*, *158*(1–4), 1–13.

Lückge, A., H. Doose-Rolinski, A. A. Khan, H. Schulz, and U. von Rad (2001), Monsoonal variability in the northeastern Arabian Sea during the past 5000 years: Geochemical evidence from laminated sediments, *Palaeogeogr. Palaeoclimatol. Palaeoecol.*, *167*(3–4), 273–286.

Lückge, A., L. Reinhardt, H. Andruleit, H. Doose-Rolinski, U. von Rad, H. Schulz, and U. Treppke (2002), Formation of varve-like laminae off Pakistan: Decoding 5 years of sedimentation, in *The Tectonic and Climatic Evolution of the Arabian Sea Region*, edited by P. D. Clift et al., pp. 421–431, Geological Society, London.

Lückge, A., G. Deplazes, H. Schulz, G. Scheeder, A. Suckow, S. Kasten, and G. H. Haug (2012), Impact of Indus River discharge on productivity and preservation of organic carbon in the Arabian Sea over the twentieth century, *Geology*, *40*(5), 399–402.

McManus, J. F., R. Francois, J. M. Gherardi, L. D. Keigwin, and S. Brown-Leger (2004), Collapse and rapid resumption of Atlantic meridional circulation linked to deglacial climate changes, *Nature*, *428*(6985), 834–837.

Middleton, N. J. (1986), Dust storms in the Middle East, *J. Arid Environ.*, *10*(2), 83–96.

Milliman, J. D., G. S. Quraishee, and M. A. A. Beg (1984), Sediment discharge from the Indus River to the Ocean: Past, present, future, in *Marine Geology and Oceanography of Arabian Sea and Coastal Pakistan*, edited by P. Haq and J. D. Milliman, pp. 65–70, van Nostrand Reinhold, New York.

Mulitza, S., M. Prange, J. B. Stuut, M. Zabel, T. von Dobeneck, A. C. Itambi, J. Nizou, M. Schulz, and G. Wefer (2008), Sahel megadroughts triggered by glacial slowdowns of Atlantic meridional overturning, *Paleoceanography*, *23*, PA4206, doi:10.1029/2008PA001637.

North Greenland Ice Core Project Members (2004), High-resolution record of Northern Hemisphere climate extending into the last interglacial period, *Nature*, *431*(7005), 147–151.

Pedersen, T. F., G. B. Shimmield, and N. B. Price (1992), Lack of enhanced preservation of organic matter in sediments under the oxygen minimum on the Oman Margin, *Geochim. Cosmochim. Acta*, *56*(1), 545–551.

Peterson, L. C., G. H. Haug, K. A. Hughen, and U. Röhl (2000), Rapid changes in the hydrologic cycle of the tropical Atlantic during the last glacial, *Science*, *290*(5498), 1947–1951.

Pichevin, L., E. Bard, P. Martinez, and I. Billy (2007), Evidence of ventilation changes in the Arabian Sea during the late Quaternary: Implication for denitrification and nitrous oxide emission, *Global Biogeochem. Cycles*, *21*, GB4008, doi:10.1029/2006GB002852.

Pourmand, A., F. Marcantonio, and H. Schulz (2004), Variations in productivity and eolian fluxes in the northeastern Arabian Sea during the past 110 ka, *Earth Planet. Sci. Rev.*, *221*(1–4), 39–54.

Preusser, F., D. Radies, and A. Matter (2002), A 160,000-year record of dune development and atmospheric circulation in southern Arabia, *Science*, *296*(5575), 2018–2020.

Prins, M. A., and G. Postma (2000), Effects of climate, sea level, and tectonics unraveled for last deglaciation turbidite records of the Arabian Sea, *Geology*, *28*(4), 375–378.

Prins, M. A., and G. J. Weltje (1999), End-member modeling of siliciclastic grain-size distributions: The Late Quaternary record of eolian and fluvial sediment supply to the Arabian Sea and its paleoclimatic significance, in *Numerical Experiments in Stratigraphy: Recent Advances in Stratigraphic and Sedimentologic Computer Simulations*, edited by J. W. Harbaugh et al., pp. 91–111, Society for Sedimentary Geology, Tulsa, USA.

Prins, M. A., G. Postma, J. Cleveringa, A. Cramp, and N. H. Kenyon (2000), Controls on terrigenous sediment supply to the Arabian Sea during the late Quaternary: The Indus Fan, *Mar. Geol.*, *169*(3–4), 327–349.

Rea, D. K. (1994), The paleoclimate record provided by eolian deposition in the deep sea: the geologic history of wind, *Rev. Geophys.*, *32*(2), 159–195.

Reichart, G. J., L. J. Lourens, and W. J. Zachariasse (1998), Temporal variability in the northern Arabian Sea Oxygen Minimum Zone (OMZ) during the last 225,000 years, *Paleoceanography*, *13*(6), 607–621.

Reichart, G. J., H. Brinkhuis, F. Huiskamp, and W. J. Zachariasse (2004), Hyperstratification following glacial overturning events in the northern Arabian Sea, *Paleoceanography*, *19*, PA2013, doi:10.1029/2003PA000900.

Roberts, A. P., E. J. Rohling, K. M. Grant, J. C. Larrasoana, and Q. S. Liu (2011), Atmospheric dust variability from Arabia and China over the last 500,000 years, *Quat. Sci. Rev.*, *30*(25–26), 3537–3541.

Rosenberg, T. M., F. Preusser, D. Fleitmann, A. Schwalb, K. Penkman, T. W. Schmid, M. A. Al-Shanti, K. Kadi, and A. Matter (2011), Humid periods in southern Arabia: Windows of opportunity for modern human dispersal, *Geology*, *39*(12), 1115–1118.

Ruth, U., M. Bigler, R. Röthlisberger, M. L. Siggaard-Andersen, S. Kipfstuhl, K. Goto-Azuma, M. E. Hansson, S. J. Johnsen, H. Y. Lu, and J. P. Steffensen (2007), Ice core evidence for a very tight link between North Atlantic and east Asian glacial climate, *Geophys. Res. Lett.*, *34*, L03706, doi:10.1029/2006GL027876.

Schefuss, E., H. Kuhlmann, G. Mollenhauer, M. Prange, and J. Pätzold (2011), Forcing of wet phases in southeast Africa over the past 17,000 years, *Nature*, *480*(7378), 509–512.

Schmittner, A., E. D. Galbraith, S. W. Hostetler, T. F. Pedersen, and R. Zhang (2007), Large fluctuations of dissolved oxygen in the Indian and Pacific oceans during Dansgaard-Oeschger oscillations caused by variations of North Atlantic Deep Water subduction, *Paleoceanography*, *22*, PA3207, doi:10.1029/2006PA001384.

Schulte, S., and P. J. Müller (2001), Variations of sea surface temperature and primary productivity during Heinrich and Dansgaard-Oeschger events in the northeastern Arabian Sea, *Geo-Mar. Lett.*, *21*(3), 168–175.

Schulte, S., F. Rostek, E. Bard, J. Rullkötter, and O. Marchal (1999), Variations of oxygen-minimum and primary productivity recorded in sediments of the Arabian Sea, *Earth Planet. Sci. Rev.*, *173*(3), 205–221.

©2014. American Geophysical Union. All Rights Reserved.

Schulz, H., U. von Rad, and H. Erlenkeuser (1998), Correlation between Arabian Sea and Greenland climate oscillations of the past 110,000 years, *Nature*, *393*(6680), 54–57.

Schulz, H., K. C. Emeis, H. Erlenkeuser, U. von Rad, and C. Rolf (2002), The Toba volcanic event and interstadial/stadial climates at the marine isotopic stage 5 to 4 transition in the northern Indian Ocean, *Quat. Res.*, *57*(1), 22–31.

Siddall, M., E. J. Rohling, W. G. Thompson, and C. Waelbroeck (2008), Marine Isotope Stage 3 sea level fluctuations: Data synthesis and new outlook, *Rev. Geophys.*, *46*, RG4003, doi:10.1029/2007RG000226.

Sinninghe Damsté, J. S., W. I. C. Rijpstra, and G. J. Reichart (2002), The influence of oxic degradation on the sedimentary biomarker record II. Evidence from Arabian Sea sediments, *Geochim. Cosmochim. Acta*, *66*(15), 2737–2754.

Sirocko, F., and H. Lange (1991), Clay-mineral accumulation rates in the Arabian Sea during late Quaternary, *Mar. Geol.*, *97*(1–2), 105–119.

Sirocko, F., and M. Sarnthein (1989), Wind-borne deposits in the northwestern Indian Ocean: Record of Holocene sediments versus modern satellite data, in *Paleoclimatology and Paleometeorology: Modern and Past Patterns of Global Atmospheric Transport*, edited by M. Leinen and M. Sarnthein, pp. 401–433, Kluwer Academic Publishers, Dordrecht.

Sirocko, F., M. Sarnthein, H. Erlenkeuser, H. Lange, M. Arnold, and J. C. Duplessy (1993), Century-scale events in monsoonal climate over the past 24,000 years, *Nature*, *364*(6435), 322–324.

Sirocko, F., D. Garbe-Schönberg, and C. Devey (2000), Processes controlling trace element geochemistry of Arabian Sea sediments during the last 25,000 years, *Global Planet. Change*, *26*(1–3), 217–303.

Stager, J. C., D. B. Ryves, B. M. Chase, and F. S. R. Pausata (2011), Catastrophic drought in the Afro-Asian monsoon region during Heinrich event 1, *Science*, *331*(6022), 1299–1302.

Stanford, J. D., R. Hemingway, E. J. Rohling, P. G. Challenor, M. Medina-Elizalde, and A. J. Lester (2011), Sea-level probability for the last deglaciation: A statistical analysis of far-field records, *Global Planet. Change*, *79*(3-4), 193–203.

Storey, M., R. G. Roberts, and M. Saidin (2012), Astronomically calibrated $^{40}Ar/^{39}Ar$ age for the Toba supereruption and global synchronization of late Quaternary records, *Proc. Natl. Acad. Sci. USA*, *109*(46), 18,684–18,688.

Stuut, J.-B. W., M. A. Prins, R. R. Schneider, G. J. Weltje, J. H. F. Jansen, and G. Postma (2002), A 300-kyr record of aridity and wind strength in southwestern Africa: Inferences from grain-size distributions of sediments on Walvis Ridge, SE Atlantic, *Mar. Geol.*, *180*(1–4), 221–233.

Sun, Y. B., S. C. Clemens, C. Morrill, X. P. Lin, X. L. Wang, and Z. S. An (2012), Influence of Atlantic meridional overturning circulation on the East Asian winter monsoon, *Nat. Geosci.*, *5*(1), 46–49.

Tyson, R. V. (2005), The "productivity versus preservation" controversy: Cause, flaws, and resolution, in *The Deposition of Organic-Carbon-Rich Sediments: Models, Mechanisms and Consequences*, edited by N. B. Harris, pp. 17–33, Society of Sedimentary Geology, Tulsa, USA.

van der Weijden, C. H., G. J. Reichart, and B. J. H. van Os (2006), Sedimentary trace element records over the last 200 kyr from within and below the northern Arabian Sea oxygen minimum zone, *Mar. Geol.*, *231*(1–4), 69–88.

von Rad, U., and M. Tahir (1997), Late Quaternary sedimentation on the outer Indus shelf and slope (Pakistan): Evidence from high-resolution seismic data and coring, *Mar. Geol.*, *138*(3–4), 193–236.

von Rad, U., H. Schulz, V. Riech, M. den Dulk, U. Berner, and F. Sirocko (1999), Multiple monsoon-controlled breakdown of oxygen-minimum conditions during the past 30,000 years documented in laminated sediments off Pakistan, *Palaeogeogr. Palaeoclimatol. Palaeoecol.*, *152*(1–2), 129–161.

von Rad, U., K.-P. Burgath, M. Pervaz, and H. Schulz (2002), Discovery of the Toba Ash (c. 70 ka) in a high-resolution core recovering millennial monsoonal variability off Pakistan, in *The Tectonic and Climatic Evolution of the Arabian Sea Region*, edited by P. D. Clift et al., pp. 445–461, Geological Society, London.

Wang, Y. J., H. Cheng, R. L. Edwards, Z. S. An, J. Y. Wu, C. C. Shen, and J. A. Dorale (2001), A high-resolution absolute-dated Late Pleistocene monsoon record from Hulu Cave, China, *Science*, *294*(5550), 2345–2348.

Wang, Y. J., H. Cheng, R. L. Edwards, X. G. Kong, X. H. Shao, S. T. Chen, J. Y. Wu, X. Y. Jiang, X. F. Wang, and Z. S. An (2008), Millennial- and orbital-scale changes in the East Asian monsoon over the past 224,000 years, *Nature*, *451*(7182), 1090–1093.

Webster, P. J., V. O. Magana, T. N. Palmer, J. Shukla, R. A. Tomas, M. Yanai, and T. Yasunari (1998), Monsoons: Processes, predictability, and the prospects for prediction, *J. Geophys. Res.*, *103*(C7), 14,451–14,510.

Weltje, G. J. (1997), End-member modeling of compositional data: Numerical-statistical algorithms for solving the explicit mixing problem, *Math. Geol.*, *29*(4), 503–549.

Wolff, E. W., J. Chappellaz, T. Blunier, S. O. Rasmussen, and A. Svensson (2010), Millennial-scale variability during the last glacial: The ice core record, *Quat. Sci. Rev.*, *29*, 2828–2838.

Wu, G., Y. Liu, B. He, Q. Bao, A. Duan, and F. F. Jin (2012), Thermal controls on the Asian summer monsoon, *Sci. Rep.*, *2*(404), doi:10.1038/srep00404.

Zhang, R., and T. L. Delworth (2005), Simulated tropical response to a substantial weakening of the Atlantic thermohaline circulation, *J. Clim.*, *18*(12), 1853–1860.

Ziegler, M., L. J. Lourens, E. Tuenter, F. Hilgen, G. J. Reichart, and N. Weber (2010), Precession phasing offset between Indian summer monsoon and Arabian Sea productivity linked to changes in Atlantic overturning circulation, *Paleoceanography*, *25*, PA3213, doi:10.1029/2009PA001884.

©2014. American Geophysical Union. All Rights Reserved.